Available online at www.sciencedirect.com
SCIENCE DIRECT®
Journal of Organometallic Chemistry 690 (2005) 1147–1156
Journal of Organometallic Chemistry
www.elsevier.com/locate/jorganchem

Density functional theory study on structural isomers and bonding of model complexes $M(CO)_5(BH_3 \cdot PH_3)$ (M = Cr, Mo, W) and $W(CO)_5(BH_3 \cdot AH_3)$ (A = N, P, As, Sb)

Alireza Ariafard [a,*], Mostafa M. Amini [*,b], Amirreza Azadmehr [b]

[a] Department of Chemistry, Faculty of Science, Central Tehran Branch, Islamic Azad University, Felestin Square, Tehran, Iran
[b] Department of Chemistry, Shahid Beheshti University, Tehran, Iran

Received 26 July 2004; accepted 11 November 2004
Available online 29 December 2004

Abstract

The influence of group 15 various substituents and effect of metal centers on metal–borane interactions and structural isomers of transition metal–borane complexes $W(CO)_5(BH_3 \cdot AH_3)$ and $M(CO)_5(BH_3 \cdot PH_3)$ (A = N, P, As, and Sb; M = Cr, Mo, and W), were investigated by pure density functional theory at BP86 level. The following results were observed: (a) the ground state is monodentate, η^1, with C_1 point group; (b) in all complexes, the η^1 isomer with C_S symmetry on potential energy surface is the transition state for oscillating borane; (c) the η^2 isomer is the transition state for the hydrogens interchange mechanism; (d) in $W(CO)_5(BH_3 \cdot AH_3)$, the degree of pyramidalization at boron, interaction energy as well as charge transfer between metal and boron moieties, energy barrier for interchanging hydrogens, and diffuseness of A increase along the series A = Sb < As < P < N; (e) in $M(CO)_5(BH_3 \cdot PH_3)$, interaction energy is ordered as M = W > Cr > Mo, while energy barrier for interchanging hydrogens decreases in the order of M = Cr > W > Mo.

Keywords: Density functional calculations; Borane complexes; Charge transfer

1. Introduction

A large number of transition metal complexes containing tetrahydroborate ligand, BH_4^-, are known. The BH_4^- ligand can bind to metal atoms in three fashions (Scheme 1), depending on number of bridging hydrogens between boron and metal center atoms [1–3].

It is well established that the BH_4^- coordination modes (η^1, η^2 and η^3) depend on the number of electrons which are offered to metal. A BH_4^- can act as 2-, 4-, or 6-electron donor, when it is bonded to the metal by η^1, η^2 or η^3 coordination modes [1,4,5]. Actually, each B–H unit donates its σ-bonding electron pair to the metal center to form a metal–ligand dative bond [1]. The BH_4^- coordination modes in some complexes can readily be understood according to the 18-electron rule. Interestingly, in these complexes the bridge H^b and terminal H^t hydrogens of BH_4^- ligand can be interchanged at ambient temperature [6].

In these complexes, the η^1 coordination modes in comparison with η^2 and η^3 ones are limited. The η^1 coordination modes are usually unstable and are converted to the other coordination modes [7,8]. Bomer et al. [9] in 1977 characterized the first stable complex of borohydride with η^1 mode, $Cu(\eta^1\text{-}BH_3OAc)(PMePh_2)_3$. Later on $M(\eta^1\text{-}BH_4)(PMePh_2)$ (M = Ag, Cu) [10,11], $Mn(\eta^1\text{-}BH_4)_3 \cdot THF$ [12], $V(\eta^1\text{-}BH_4)_2(dmpe)_2$ [13,14], $FeH(\eta^1\text{-}BH_4)(dmpe)_2$ [15], $CpMn(CO)_2(\eta^1\text{-}BH_3 \cdot L)$ (L = NMe_3 and PMe_3) [16],

* Corresponding author. Tel.: 98 21 4803708; fax: 98 281 2563931.
E-mail address: ariafard@yahoo.com (A. Ariafard).

0022-328X/$ - see front matter © 2004 Elsevier B.V. All rights reserved.
doi:10.1016/j.jorganchem.2004.11.021

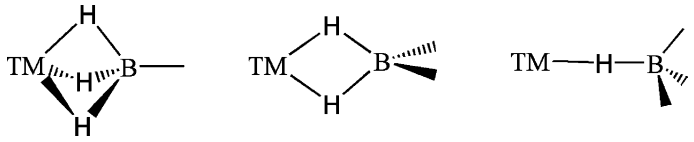

Scheme 1.

and $Mn(CO)_4$- $(PMe_2Ph)(\eta^1\text{-}BH_3 \cdot L)$ [17] with η^1 coordination mode were reported. The formal oxidation states of metals in above-mentioned complexes are +1, +2 or +3. However, recently Shimoi and coworkers synthesized borohydride complexes with η^1 coordination mode in which the metal oxidation states are zero [18,19]. They reported that photolysis of $M(CO)_6$ (M = Cr, Mo, and W) in presence of $B_2H_6 \cdot 2PMe_3$ and $BH_3 \cdot L$ (L = PMe_3, PPh_3, NMe_3) ligands generates $M(CO)_5(\eta^1\text{-}B_2H_4 \cdot 2L)$ and $M(CO)_5(\eta^1\text{-}BH_3 \cdot L)$. The structures of W and Cr analogues have been determined by X-ray diffraction analysis, whereas Mo derivatives thermally are unstable and have only been characterized by NMR spectroscopy. Interestingly, for large number of $M(CO)_5(\eta^1\text{-}BH_3 \cdot L)$ complexes only a single peak was observed in their ^1H NMR spectrum from room temperature down to −80 °C, indicating that the coordinated H_b and terminal H_t are rapidly exchanging in solution. As a contribution to this interesting class of compounds, this paper details with structural and electronic features of $M(CO)_5(\eta^1\text{-}BH_3 \cdot AH_3)$ complexes as models for the real complexes. In addition, we have studied the effect of central metal as well as A atom on energy barrier for scrambling between terminal and bridge hydrogens.

2. Computational details

Geometry optimizations were performed at BP86 level [20] of density functional theory for all model complexes in which methyl groups are replaced by hydrogen atoms for theoretical simplicity. The geometries of different species under consideration were optimized using analytic gradient. The harmonic vibrational frequencies of the different stationary points of the PES have been calculated at the same level of theory in order to identify the local minima as well as to estimate the corresponding zero point vibrational energy (ZPE).

The 6-31G** was used for BH_3 moiety. Other hydrogen atoms, carbons and oxygens were described with standard 6-31G basis set [21]. The LANL2DZ effective core potentials [22] and basis sets were used to describe transition metals, phosphorus, arsenic, and antimony. All calculations were performed using the GAUSSIAN 98 software package [23].

The natural bond orbital (NBO) [24] theory was used to evaluate the bond hybridization and Wiberg bond indices [25]. The energies associated with charge transfer and particular orbital interaction were calculated with the NBO deletion procedure as the difference between the total SCF energy and the energy obtained by deleting the off-diagonal Fock matrix elements corresponding to interacting filled–unfilled orbital [24]. NBO calculations were performed with NBO code [26] included in GAUSSIAN 98.

The final interaction energies, $E_{I+BSSE}(AB)$, have been calculated as difference between the energy of the complex and sum of the energies of the monomers ($M(CO)_5$ and $BH_3 \cdot AH_3$). These values have been corrected from the inherent basis set superposition error (BSSE) which is calculated, using the Boys–Bernardi counterpoise technique [27]

$$E_{I+BSSE}(AB) = E(AB)_{AB} - E(A)_A - E(B)_B + [E(A')_A - E(A')_{AB}] + [E(B')_B - E(B')_{AB}]$$

where $E(AB)_{AB}$ represents the energy of complex, $E(A)_A$ the energy of the isolated monomer A with its basis set, $E(A')_A$ the energy of A in its geometry within the complex calculated with its basis set, and $E(A')_{AB}$ the energy of A in its geometry within the complex with the complete basis set of the complex AB.

3. Results and discussion

3.1. Investigation of electronic properties of $W(CO)_5(BH_3 \cdot AH_3)$ (A = N, P, As and Sb) complexes

In order to see the effect of types of A atoms on electronic features of $W(CO)_5(BH_3 \cdot AH_3)$ (A = N, P, As and Sb) model complexes, the corresponding structures have been fully optimized at BP86 level (Scheme 2). The selected structural data for the calculated complexes are represented in Table 1. For $\mathbf{W_P}$, the optimized geometries obtained from above calculations are in satisfactory agreement with the experimental values [19] of $W(CO)_5(BH_3 \cdot PMe_3)$ complexes (Table 1). However, it should be mentioned that the only discrepancies are found in the B–H and W–H bond distances. These discrepancies can be attributed to the systematic error resulting from positions of hydrogen atoms in X-ray

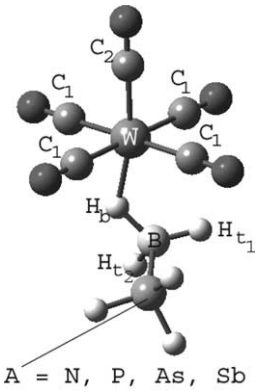

W_A

C_1 Symmetry

W_N : A = N

W_P : A = P

W_{As} : A = As

W_{Sb} : A = Sb

Scheme 2.

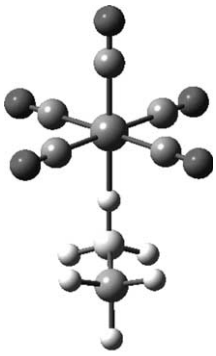

W'_A

C_s Symmetry

Scheme 3.

diffraction studies of these complexes. The optimized structure of $\mathbf{W_N}$–$\mathbf{W_{Sb}}$ can be described as an octahedral geometry. For all complexes, as most stable conformations, C_1 symmetries were obtained in which borane is bonded to central metal as a η^1 mode. This result is in excellent agreement with experimental data. The η^1 mode with C_s symmetry (Scheme 3) has an imaginary frequency; indicating $\mathbf{W'_A}$ is not a ground state. Examining results of frequency calculations, we found that $\mathbf{W'_A}$ can be a transition state for exchange of $BH_3 \cdot AH_3$ ligand from side to side in the complexes. Also, the energy differences between conformations $\mathbf{W'_A}$ and $\mathbf{W_A}$ are so much small that it seems the borane can readily oscillate in room temperature and lower (1.1 kcal/mol for $\mathbf{W_N}$, 2.1 kcal/mol for $\mathbf{W_P}$, 1.9 kcal/mol for $\mathbf{W_{As}}$, and 2.1 kcal/mol for $\mathbf{W_{Sb}}$). In addition, the vibration frequency study of the complexes in the ground state indicates that there is a harmonic motion with very small frequency, corresponding to the rotation of the η^1-$BH_3 \cdot AH_3$ along the W–B axes. This indicates that the $BH_3 \cdot AH_3$ rotational barrier along the W–B axes is very small. Such feature for a number of tetrahydroborate complexes has also been reported [28,29], in which the rotational barrier of borohydride ligand along metal–BH_4 axes is explained based on the very low energy value of the corresponding vibrational mode.

Regarding the metal–BH_4 bonding feature in this type of complexes, Parry and Kodama [30] have suggested that the B–H has ability to donate the σ-bonding pair, to some extent, to central metal and make a 3c–2e bond. The σ-bonding electron donation feature of B–H can be easily seen in $\mathbf{W_N}$–$\mathbf{W_{Sb}}$ in which B–H_b bond distances are significantly longer than B–H_t bond distances. Table 1 clearly shows that the calculated bond distances of B–H_b for all complexes are within the range of 1.262–1.282 Å, while those of B–H_t bonds are within range of 1.201–1.213 Å. The NBO analyses also show that bond orders of W–H_b are significantly larger than those of W–H_t (Table 2). In addition to this electronic feature, NBO analyses confirm that W–B bonding interactions for all complexes are present in which the Wiberg bond indices of W–B are within the range of 0.113–0.115. In view of the structural and electronic characteristics described above, one can conclude that these complexes are as η^1 coordination modes.

Taking into account Parry and Kodama [30] suggestion, one expects that the electron occupancy of B–H_b bond can be a good indication of the extent of its electron

Table 1
Selected optimized geometrical parameters (Å, °) for $W(CO)_5(BH_3 \cdot AH_3)$ (A = N, P, As, Sb) model complexes and experimental ones for $W(CO)_5(BH_3 \cdot PMe_3)$ complex

Species	W–C_1 (average)	W–C_2	W–H_b	B–H_b	B–H_{t1}	B–H_{t2}	B–W	$\sum\theta$	$\sum\theta'$
W_N	2.035	1.987	1.930	1.282	1.205	1.213	2.905	326.7	333.6
W_P	2.037	1.981	1.955	1.266	1.203	1.211	2.860	303.8	339.8
W_{As}	2.037	1.981	1.951	1.265	1.202	1.209	2.874	300.1	340.4
W_{Sb}	2.038	1.980	1.958	1.262	1.201	1.207	2.852	294.7	345.0
[W(CO)5(BH3 · PMe3)][a]	2.05(2)	1.97(1)	2.01(9)	1.14(10)	0.92(12)	1.14(28)	2.86(2)	–	–

[a] Ref. [19].

Table 2
Selected calculated Wiberg bond indices (from NBO) for $W(CO)_5(BH_3 \cdot AH_3)$ (A = N, P, As, Sb)

Species	W–C_1 (average)	W–C_2	W–H_b	W–H_{t1}	W–H_{t2}	B–H_b	B–H_{t1}	B–H_{t2}	B–W
W_N	0.880	1.114	0.157	0.003	0.006	0.721	0.978	0.967	0.113
W_P	0.872	1.140	0.137	0.004	0.004	0.757	0.961	0.953	0.114
W_{As}	0.870	1.141	0.139	0.004	0.005	0.756	0.964	0.953	0.113
W_{Sb}	0.868	1.145	0.134	0.004	0.004	0.766	0.965	0.959	0.115

donation to central metal. The electron occupancy of B–H_b σ-bonding was calculated by NBO analyses and results are listed in Table 3. Results of calculations indicate that the σ-bonding electron donation of B–H_b decreases in the order of $\mathbf{W_N > W_p \approx W_{As} > W_{Sb}}$. A similar trend is also visible in bond order and bond distance of B–H_b (Tables 1 and 2).

3.2. Charge transfer

It seems that reduction of electron density in σ-bond of B–H_b in comparison with that in B–H_t can be a good criterion for measuring charge transferred from $BH_3 \cdot AH_3$ to $W(CO)_5$. Since charge transfer interactions are associated with the occupancy shifts from the manifold of filled orbitals of one fragment to the unfilled orbitals of other, ΔE_{CT} can be estimated by deleting Fock matrix elements connecting these manifolds and noting to the total energy. In the present work, by using this approach, the energies of charges transferred between $W(CO)_5$ and $BH_3 \cdot AH_3$ species have been calculated and results are given in Table 3. The charge transfers are predominately in the direction from $BH_3 \cdot AH_3$ to $W(CO)_5$. The largest single contribution to ΔE_{CT} can be identified with the matrix element $\langle \sigma_{B-Hb} | F | \sigma^*_{W-C2} \rangle$ between the σ_{B-Hb} of donor $BH_3 \cdot AH_3$ ligand and unfilled antibonding σ* of acceptor $W(CO)_5$ fragments. When this single element of Fock matrix is set to zero and all other elements are left unchanged, the donated energies are obtained, which are 109.5, 95.0, 94.1 and 92.8 kcal/mol for $\mathbf{W_N}$, $\mathbf{W_P}$, $\mathbf{W_{As}}$, and $\mathbf{W_{Sb}}$, respectively. The results confirm that the charge is mainly in direction from σ_{B-Hb} to σ^*_{W-C2} and there is no back-donation from $M(CO)_5$ to $BH_3 \cdot AH_3$ ligand.

On the basis of molecular orbital theory the σ^*_{W-C2} is only a slight W–C σ-antibonding orbital which has proper symmetry for interaction with the B–H σ-bonding orbital of $BH_3 \cdot AH_3$ ligand (Scheme 4). It is evident that a rise in the extent of the charge transferred from $BH_3 \cdot AH_3$ to $W(CO)_5$ makes the W–C2 interaction weaker. This effect clearly explains why the W–C2 bond distance in $\mathbf{W_N}$ is slightly longer than that in other complexes.

To understand above electronic behavior we have defined two geometrical parameters (Scheme 5): (a) the sum of the bond angles around A, $\sum\theta = \theta_1 + \theta_2 + \theta_3$ and (b) around B, $\sum\theta' = \theta'_1 + \theta'_2 + \theta'_3$, which measure the degree of pyramidalization at them (Table 1). It is clear from this table that the $\mathbf{W_N}$ complex has the largest $\sum\theta$ among these complexes, and that decreases along the series from $\mathbf{W_N}$ to $\mathbf{W_{Sb}}$. This trend can be rationalized in terms of increasing p character in the A–H σ-bonds as one moves down group 15 from N to Sb (the calculated p/s ratios for the A–H σ-bonds are 3.57 in $\mathbf{W_N}$, 3.86 in $\mathbf{W_P}$, 3.92 in $\mathbf{W_{As}}$, and 3.94 in $\mathbf{W_{Sb}}$). As a result, lone electron pair on A have more p-character when moving up the column, similar to the well-known behavior of NH_3 versus PH_3 [31]. This behavior is also in accordance with Bent's rule [32]. By increasing p-character of lone pair on A, slightly its diffuseness and overlap with acceptor fragment increase. Thus, electron donor ability of NH_3 in $BH_3 \cdot NH_3$ is more significant than that of AH_3 (A = P, As, and Sb) in other complexes. Apparently, the increase of diffuseness of lone pair on A causes an increase in the degree of pyramidalization at BH_3. The sum of the bond angles around B (Scheme 5), $\sum\theta'$, can be an appropriate criterion for determining the degree of pyramidalization. In $W(CO)_5(BH_3 \cdot AH_3)$ complexes, the values of $\sigma\theta'$ are ordered as $\mathbf{W_N}$ (333.6°) < $\mathbf{W_P}$ (339.8°) < $\mathbf{W_{As}}$ (340.4°) < $\mathbf{W_{Sb}}$ (345.0°). The higher pyramidalization degree of BH_3 leads to an increase in p-character in B–H bonds. In addition, the results of calculations indicate that the boron p/s ratios of B–A bonds are 4.47, 4.71, 5.15, and 6.44 for the complexes $\mathbf{W_N}$, $\mathbf{W_P}$, $\mathbf{W_{As}}$,

Table 3
Natural bond occupancies for σ_{B-H} orbitals and deleting Fock matrix elements (kcal/mol) between $M(CO)_5$ and $BH_3 \cdot AH_3$ fragment as well as σ_{B-Hb} filled orbital and σ^*_{W-C2} unfilled orbital within $[W(CO)_5(BH_3 \cdot AH_3)]$ model complexes

Species	σ_{B-H_b}	$\sigma_{B-H_{t1}}$	$\sigma_{B-H_{t2}}$	ΔE_{CT} $M(CO)_5 \cdots BH_3 \cdot AH_3$	$\langle \sigma_{B-Hb} \mid F \mid \sigma^*_{W-C2} \rangle$
W_N	1.746	1.981	1.971	111.0	109.5
W_P	1.771	1.965	1.961	100.7	95.0
W_{As}	1.771	1.982	1.968	100.6	94.1
W_{Sb}	1.781	1.969	1.967	99.3	92.8

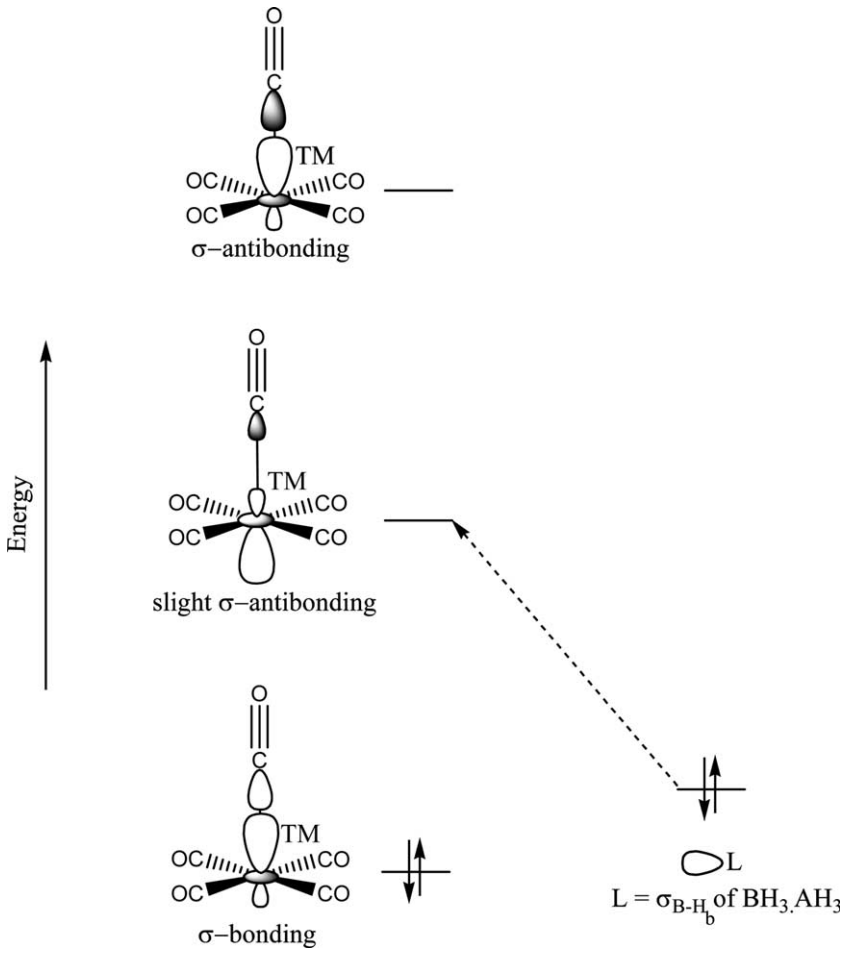

Scheme 4.

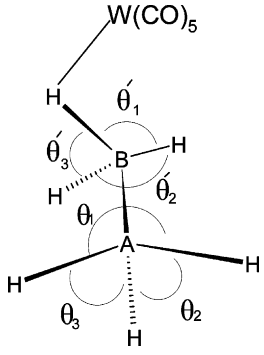

Scheme 5.

and $\mathbf{W_{Sb}}$, respectively. Therefore, it should be concluded that diminishing contribution of boron p orbital in A–B bond is resulted in increasing same contribution, p, in B–H bonds. In such case, B–H σ-bonding orbital in $BH_3 \cdot AH_3$ with more diffuse A, such as the expression containing nitrogen, should have higher energy than other ones. Therefore the B–H σ-bonding orbital and the slight W–C2 σ-antibonding orbital in $\mathbf{W_N}$ should be closer in energy, leading to a more effective interaction.

3.3. Interaction energy between $W(CO)_5$ and $BH_3 \cdot AH_3$

The results obtained from the interaction energy between $W(CO)_5$ and $BH_3 \cdot AH_3$ in the optimized complexes are given in Table 4. Our effort for optimizing $BH_3 \cdot SbH_3$ in BP86 level was not successful; therefore, we couldn't report interaction energy in $\mathbf{W_{Sb}}$. Generally, the BSSE effect is not very significant in all the cases. In terms of energy, the complex formed between $W(CO)_5$ and $BH_3 \cdot NH_3$ is the most stable complex in these series, which is in satisfactory agreement with the results obtained from its charge transfer. The strength of interaction between $BH_3 \cdot AH_3$ and $W(CO)_5$ fragments is ordered as following: $\mathbf{W_N > W_P > W_{As}}$. It is interesting to note that, in these series of complexes, though $BH_3 \cdot PH_3$ and $BH_3 \cdot AsH_3$ ligands have fairly similar transferred charge to $W(CO)_5$ (see ΔE_{CT} in Table 3), the interaction of $BH_3 \cdot PH_3$ with central metal is somewhat stronger than that of $BH_3 \cdot AsH_3$ with metal center. Since the interaction energy contains charge transfer (CT) and no-charge transfer (NCT) parts, interaction energy = $\Delta E_{NCT} + \Delta E_{CT}$ [24], the difference between them can be attributed to higher contribution of

Table 4
Interaction energies between $W(CO)_5$ and $BH_3 \cdot AH_3$ fragments without (E_I) and with the BSSE correction (E_{I+BSSE}) (kcal/mol) for some of studied complexes

	E_I	BSSE	E_{I+BSSE}
$W(CO)_5 \cdots BH_3 \cdot NH_3$	31.0	3.5	27.5
$W(CO)_5 \cdots BH_3 \cdot PH_3$	24.1	2.8	21.3
$W(CO)_5 \cdots BH_3 \cdot AsH_3$	22.4	2.7	19.7

ΔE_{NCT} in the larger ligand of $BH_3 \cdot AsH_3$. In other words, the shares of repulsion and electrostatic interactions between $W(CO)_5$ and $BH_3 \cdot AsH_3$ in $\mathbf{W_{As}}$, due to larger size of $BH_3 \cdot AsH_3$ relative to $BH_3 \cdot PH_3$, are greater than those in $\mathbf{W_P}$.

Shimoi et al. [19] also showed that coordination of $BH_3 \cdot AH_3$ (A = N and P) to metal is very weak in which borane is readily dissociated and a precipitation of $W(CO)_6$ is formed in a solution containing free CO. The total interaction energy for coordination of $BH_3 \cdot NH_3$ and $BH_3 \cdot PH_3$ ligands to $W(CO)_5$ fragments, as calculated by DFT/BP86, are 27.5 and 21.3 kcal/mol, respectively (Table 4). These values can be compared with those calculated for CO coordinated to $W(CO)_5$ using same theoretical procedure (E_{I+BSSE} of 46.2 for complexation of CO). Therefore, one can conclude that the strength of interaction between $BH_3 \cdot AH_3$ and $W(CO)_5$ in the ground sate is significantly weaker than the strength of interaction between CO and $W(CO)_5$. This is in good agreement with experimental data that shows $W(CO)_5(BH_3 \cdot L)$ is easily converted to $W(CO)_6$.

3.4. η^2 coordination mode of $BH_3 \cdot AH_3$ to $W(CO)_5$

As mentioned in Section 1, the bridge H_b and terminal H_t in $[M(CO)_5(BH_3 \cdot L)]$ (M = Cr, Mo and W; L = $P(CH_3)_3$ and $N(CH_3)_3$) can be interchanged down to −80 °C, indicating that the energy barrier for exchanging process is significantly low. This result prompted us to determine a suitable transition state for the process. For all complexes, only a bidentate structure with C_s point group was calculated (Scheme 6). One imaginary frequency obtained from calculations confirms that these structures are transition state on the potential energy surfaces. The associated mode essentially corresponds to a $\eta^2 \rightarrow \eta^1$ change of the η^2-coordinated borane group; therefore, these structures are the transition states for exchange of hydrogen atoms.

The selected structural data for optimized transition states is represented in Table 5. It is clear that the W–C2 bond distance in $\mathbf{W''_A}$ in comparison with that in $\mathbf{W_A}$ decreases (Table 1). It seems that in this case the strength of σ-donation of borane to slight W–C2 σ-antibonding orbital become weaker. To calculate the extent of charge transferred from $BH_3 \cdot AH_3$ to $W(CO)_5$, we used the NBO deleting approach. The ΔE_{CT} for $\mathbf{W''_N}, \mathbf{W''_P}, \mathbf{W''_{As}}$, and $\mathbf{W''_{Sb}}$ are 84.5, 76.4, 75.8 and 76.1 kcal/mol, respectively, which shows a significant decrease compared with their corresponding results in ground state (Table 3).

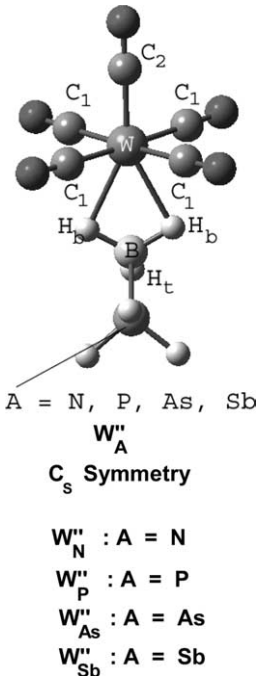

Scheme 6.

Table 5
Selected optimized geometrical parameters (Å) for transition states of $W(CO)_5(\eta^2\text{-}BH_3 \cdot AH_3)$ model complexes

Species	W–C_1	W–C_2	W–H_b	B–H_b	B–H_t	B–W
W''_N	2.038	1.968	2.367	1.226	1.210	2.757
W''_P	2.039	1.965	2.371	1.223	1.207	2.764
W''_{As}	2.039	1.965	2.376	1.222	1.206	2.763
W''_{Sb}	2.039	1.965	2.380	1.221	1.206	2.755

To further evaluate bonding features of the bidentate structures, we also used NBO analysis (Table 6). The calculated Wiberg bond indices indicate that there is a reasonable interaction between $BH_3 \cdot AH_3$ ligand and tungsten central metal. However, the W–H_b and W–B Wiberg bond indices for all the model complexes are smaller than the ones of our previous calculations for $[Mo(CO)_4(\eta^2\text{-}BH_4)]^-$ (0.133 and 0.262) and $[Cr(CO)_4(\eta^2\text{-}BH_4)]^-$ (0.141 and 0.292) [33]. From this

Table 6
Selected calculated Wiberg bond indices (from NBO) for the transition states of $W(CO)_5(BH_3 \cdot AH_3)$ model complexes

Species	W–H_b	W–H_t	W–B
W''_N	0.040	0.002	0.216
W''_P	0.035	0.001	0.195
W''_{As}	0.034	0.001	0.194
W''_{Sb}	0.034	0.001	0.194

Table 7
Relative energies without zero-point energy (ZPE) (ΔE) and with ZPE (ΔE_0) (kcal/mol) for hydrogen exchange processes within $W(CO)_5(B-H_3 \cdot AH_3)$ model complexes

	ΔE	ΔE_0
$W_N \rightarrow W''_N$	5.9	5.5
$W_P \rightarrow W''_P$	4.2	3.7
$W_{As} \rightarrow W''_{As}$	3.5	3.1
$W_{Sb} \rightarrow W''_{Sb}$	3.4	3.0

comparison we conclude that the W–borane interactions in the bidentate transition states $[W(CO)_5(\eta^2\text{-}BH_3 \cdot AH_3)]$ are weaker than those in the molybdenum and chromium borane complexes, which are minimum on the potential energy surface.

Our calculations indicate that all saddle points are located in the energy range of 3.4–5.9 kcal/mol above the local minimum, and by taking into account zero point energy (ZPE) the corresponding relative energies fall in the energy rang of 3.0–5.5 kcal/mol. Table 7 represents required energies for $\eta^2 \rightarrow \eta^1$ process for all model complexes. The results of calculations explain why coalescence can not be experimentally observed in the temperature range studied (<7.2 kcal/mol) [16]. Table 7 also shows that the calculated energy barriers for interchange of hydrogen atoms in the studied complexes decrease along the series $\mathbf{W_N > W_P > W_{As} > W_{Sb}}$. The trend can be attributed to the extent of interaction between $W(CO)_5$ and $BH_3 \cdot AH_3$. Indeed, the strong bonding interactions between them increase stability of stable species, $\mathbf{W_A}$, more than the corresponding transition states. Interestingly, these results are consistent with experimental finding for $CpMn(CO)_2(\eta^1\text{-}BH_3 \cdot L)$ (L = NMe_3, PMe_3) complexes in which the barrier for scrambling between coordinated and terminal BH hydrogens of $CpMn(CO)_2(\eta^1\text{-}BH_3 \cdot NMe_3)$ is substantially higher than that of $CpMn(CO)_2(\eta^1\text{-}BH_3 \cdot PMe_3)$ ($\Delta G^{\ddagger} = 9.6$ kcal/mol for $CpMn(CO)_2(\eta^1\text{-}BH_3 \cdot NMe_3)$ and $\Delta G^{\ddagger} = 7.2$ kcal/mol for $CpMn(CO)_2(\eta^1\text{-}BH_3 \cdot PMe_3)$) [16].

3.5. Molecular orbital calculation

The studied complexes can be formally described as d^6 species. The molecular orbital calculation of $W(CO)_5(BH_3 \cdot PH_3)$ model complex shows that the three orbitals which accommodate the six d electrons correspond to three highest occupied molecular orbitals (HOMOs), as shown in left hand column of Fig. 1. These three orbitals HOMO, HOMO − 1, and HOMO − 2 are designated as d_-, d_+, and d_{xy}, respectively. The d_- orbital represents the linear combination of $d_{xz} - d_{yz}$, while the d_+ orbital represents the linear combination of $d_{xz} + d_{yz}$. The HOMO indicates slightly a π-antibonding interaction between metal and $BH_3 \cdot AH_3$, whereas there is no significant interaction between them in HOMO − 1 and HOMO − 2. The LUMO is also represented within left hand column of Fig. 1. This unoccupied orbital is a hybrid type orbital (hy) for metal and has significant σ-antibonding character with respect to the $W–BH_3 \cdot AH_3$ bond. This result demonstrates that bonding between the borane and metal can be only described as donation of bonding electron pair of B–H to $W(CO)_5$ fragment. This is in satisfactory agreement with the results obtained from NBO analyses. Fig. 1 also exhibits the orbitals correlation diagram of HOMO − 2, HOMO − 1, HOMO and LUMO between conformations $\mathbf{W_P}$ and $\mathbf{W''_P}$. Examination of other model complexes gives similar results as well. Considering listed values in Fig. 1, one can observe that the orbital energies of HOMO − 2, HOMO − 1, and LUMO in $\mathbf{W_P}$ with respect to those analogues in $\mathbf{W''_P}$ are almost same, whereas HOMO undergoes a rise in energy when borane has a η^2 arrangement ($\mathbf{W''_P}$). Apparently, in $\mathbf{W''_P}$, there is a stronger antibonding interaction between d_- and π-orbital of borane, which leads to a greater instability in HOMO. This can be explained on the basis of the fact that the involved hydrogen atoms in antibonding interaction in average become closer to central metal (2.946 Å for $\mathbf{W_P}$ vs. 2.367 Å for $\mathbf{W''_P}$). Therefore, it is expected that the destabilization of conformations $\mathbf{W''_A}$ relative to $\mathbf{W_A}$ is related to a rise in HOMO energy.

We now understand why in comparison with $[Mo(CO)_4(\eta^2\text{-}BH_4)]^-$ and $[Cr(CO)_4(\eta^2\text{-}BH_4)]^-$ [33], the bonding interaction between $W(CO)_5$ and $AH_3 \cdot BH_3$ in $W(CO)_5(\eta^2\text{-}BH_3 \cdot AH_3)$ complexes is meaningfully weaker. In the η^2 complexes, there are no π-interaction between $W(CO)_5$ and $BH_3 \cdot AH_3$ because the d_- orbital having appropriate symmetry for π-interaction is occupied. Thus, in the bidentate transition states, the $W–AH_3 \cdot BH_3$ σ-interaction plays most important role for managing bonding while in $[M(CO)_4(\eta^2\text{-}BH_4)]^-$ (M = Cr, Mo) complexes, both σ- and π-interactions appear to be significant.

3.6. Effect of metal center

In order to investigate effect of metal center on electronic feature of these types of complexes, $Mo(CO)_5(BH_3 \cdot PH_3)$ ($\mathbf{Mo_P}$) and $Cr(CO)_5(BH_3 \cdot PH_3)$ ($\mathbf{Cr_P}$) (Scheme 7) were optimized at BP86 level. The geometries of these complexes in the ground state are similar to $\mathbf{W_P}$. Selected optimized geometrical parameters for these complexes along with experimental ones [19] for $Cr(CO)_5(BH_3 \cdot P(CH_3)_3)$ are represented in Table 8. The theoretical calculations fairly well reproduce the experimental results.

Total interaction energies between $M(CO)_5$ (M = Cr, Mo) and $BH_3 \cdot PH_3$ are listed in Table 9. From Tables 7 and 9, one can find that the total interaction energies are

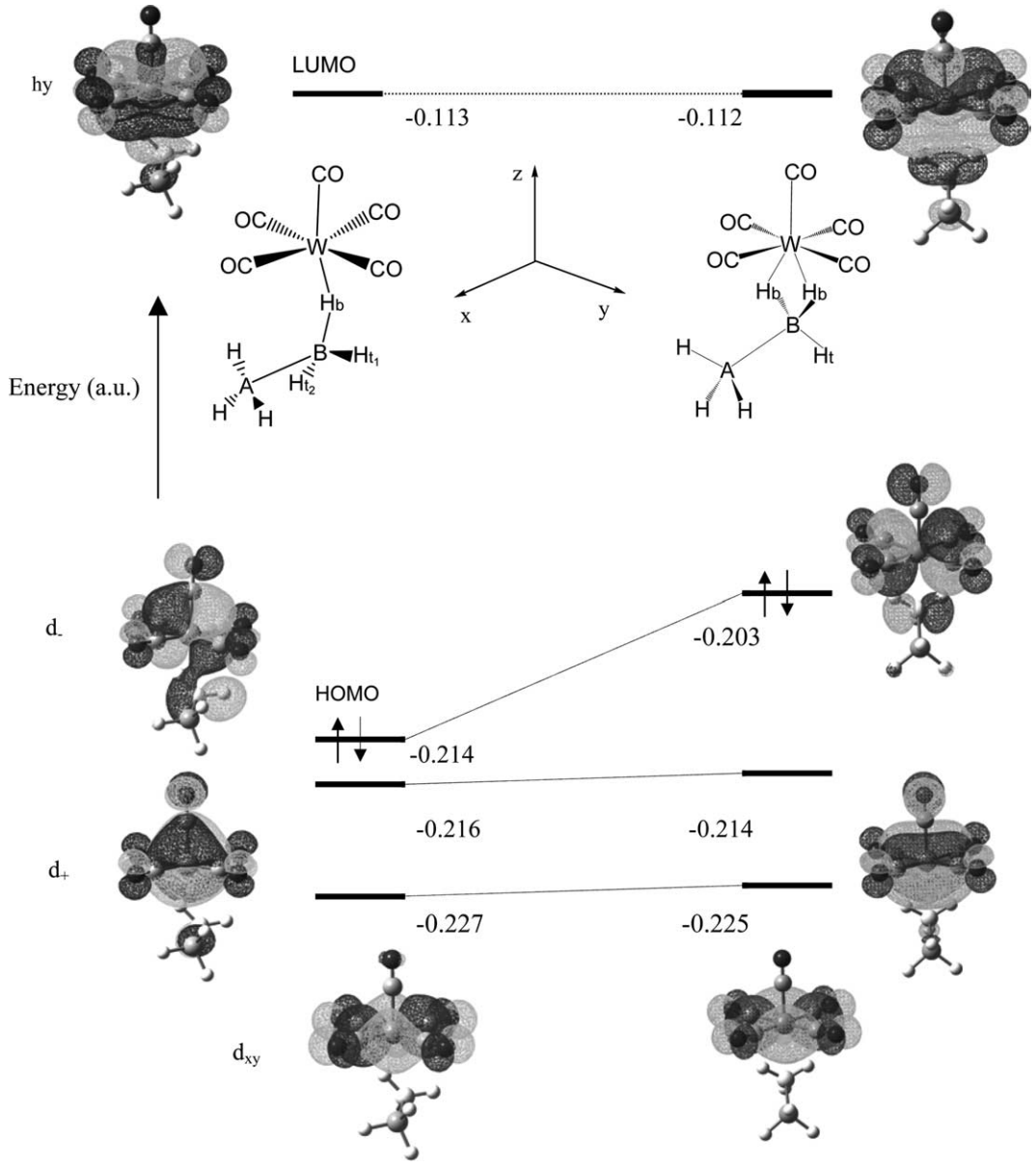

Fig. 1. Three highest occupied molecular orbitals and lowest unoccupied molecular orbital in W_P and W''_P as well as schematic showing orbital correlation diagram between them.

ordered as $\mathbf{W_P > Cr_P > Mo_P}$. This trend is in excellent accord with a rule for transition metals [34], in which the metal–ligand interaction energy changes in the following sequence: first row > second row < third row. The stronger metal–ligand bonding of the first row transition metals compared with that of the second row can be rationalized on the basis of the fact that the overlaps of the first row metal 4s orbitals with ligand orbitals are larger than the ones of the second row 5s orbitals [34]. Indeed, first row transition metals would make better interaction with ligands since radii ratio of 4s/3d is significantly larger than that of 5s/4d [35]. This behavior demonstrates that the dominant contribute in the hybridization of 3d and 4s orbitals is the metal 4s orbital. On the other hand, the larger magnitude of d orbitals of third row transition metals in metal–ligand bonding should be a plausible explanation for the fact that the metal–ligand interactions of third row transition metals are stronger than the ones of the second row analogues. For heavier transition metals, s^1d^{n+1} and s^0d^{n+1} electronic arrangements are energetically not very much greater, sometimes even smaller, than the s^2d^n ones. Furthermore, the size of d orbitals, relative to the s orbital, increases as the metal become heavier. These factors result in better s–d hybridization and larger involvement of d orbitals in metal–ligand interaction of heavier transition metal. In addition, because tungsten has more diffuse d orbitals than molybdenum,

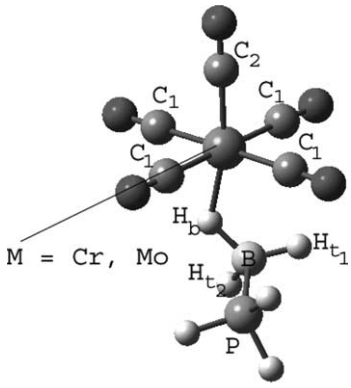

C_1 Symmetry

Cr_P : M = Cr

Mo_P : M = Mo

Scheme 7.

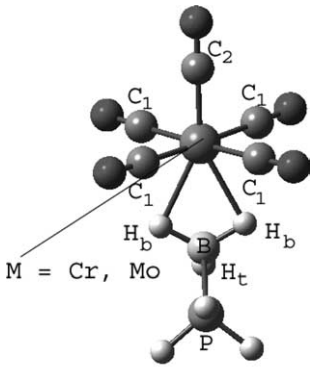

C_S Symmetry

Cr''_P : M = Cr

Mo''_P : M = Mo

Scheme 8.

it is evident that the W–ligand interactions become stronger.

The η^2 isomers of these model complexes have also been optimized at BP86 level (Scheme 8) and the important structural parameters are listed in Table 10. In view of the fact that only σ-interaction governs the W–$BH_3 \cdot AH_3$ bonding in the bidentate transition states, it is reasonable to see that the calculated metal–boron interatomic distances in $\mathbf{Cr''_P}$ (2.728 Å) and $\mathbf{Mo''_P}$ (2.798 Å) are longer than the isolated ones in $[Cr(CO)_4(\eta^2\text{-}BH_4)]^-$ (2.29 Å) [8] and $[Mo(CO)_4(\eta^2\text{-}BH_4)]^-$ (2.413 Å) [7]. This result is also supported from comparison between the calculated complexes $M(CO)_5(\eta^2\text{-}BH_3 \cdot AH_3)$ and Weller's η^2-borane complex $[(COD)Rh\{(\eta^2\text{-}BH_3)Ph_2PCH_2PPh_2\}]^+$ [36] in which the metal–boron interatomic distance in Weller's complex (2.313 Å) is significantly shorter than the ones in calculated complexes (see Tables 5 and 10).

Taking into account the results derived from the interaction energy between $M(CO)_5$ and $BH_3 \cdot PH_3$ fragments, one can expect that the energy barrier for exchanging H^b and H^t decreases in the order of $\mathbf{W_P > Cr_P > Mo_P}$. On the contrary, the results of our calculations, however, anticipate that the corresponding energy barrier increases in the following order: $\mathbf{Mo_P < W_P < Cr_P}$ (see Tables 7 and 11). It seems that the corresponding difference can be related to the increasing steric interaction between metal and boron moieties in η^2 isomer relative to that of η^1 ones. Apparently, the steric repulsive interaction in chromium complex should be significantly larger than that in tungsten complex, since in former case, boron and central metal are much closer to each other. As a result, the energy barrier for exchanging hydrogen atoms in these types of complexes is governed by both electronic and steric factors. These results are consistent with available experimental findings for similar complexes i.e., $M(CO)_5(\eta^1\text{-}B_2H_4 \cdot 2PMe_3)$(M = Cr, W), in which the free energy of

Table 8
Selected optimized geometrical parameters (Å) for $M(CO)_5(BH_3 \cdot PH_3)$ (M = Mo, Cr) model complexes and experimental ones for $Cr(CO)_5(BH_3 \cdot PMe_3)$ complex

Species	M–C_1 (average)	M–C_2	M–H_b	B–H_b	B–H_{t1}	B–H_{t2}	B–M
M = Mo(Mo_P)	2.043	1.979	1.966	1.256	1.204	1.210	2.926
M = Cr(Cr_P)	1.880	1.834	1.797	1.260	1.203	1.211	2.817
$[Cr(CO)_5(BH_3 \cdot PMe_3)]$	1.90(1)	1.84(1)	1.94(10)	1.12(11)	0.94(7)	0.97(17)	2.79(1)

Table 9
Interaction energies between $M(CO)_5$ (M = Mo, Cr) and $BH_3 \cdot PH_3$ fragments without (E_I) and with the BSSE correction (E_{I+BSSE}) (kcal/mol)

	E_I	BSSE	E_{1+BSSE}
$Mo(CO)_5 \cdots BH3 \cdot PH_3$	20.0	2.6	17.4
$Cr(CO)_5 \cdots BH3 \cdot PH_3$	19.1	2.3	16.8

Table 10
Selected optimized geometrical parameters (Å) for transition states of $M(CO)_5(\eta^2\text{-}BH_3 \cdot PH_3)$ (M = Mo, Cr) model complexes

Species	M–C_1 (Average)	M–C_2	M–H_b	B–H_b	B–H_t	B–M
$M = Mo(Mo''_P)$	2.046	1.962	2.401	1.223	1.208	2.798
$M = Cr(Cr''_P)$	1.885	1.823	2.341	1.221	1.209	2.728

Table 11
Relative energies without zero-point energy (ZPE) (ΔE) and with ZPE (ΔE_0) (kcal/mol) for hydrogen exchange within $M(CO)_5(BH_3 \cdot PH_3)$ (M = Mo, Cr) model complexes

	ΔE	ΔE_0
$Mo_P \rightarrow Mo''_P$	2.7	2.3
$Cr_P \rightarrow Cr_P$	5.4	4.8

activation for the geminal hydrogen exchange was estimated to be 6.7 kcal/mol for Cr complex, whereas activation energy for W complex, ought to be less than 6.7 kcal/mol [37].

Acknowledgement

The support of SGS cooperation gratefully acknowledged. A. Ariafard thanks Professor Zhenyang Lin, Hong Kong University of Science and Technology, for their fruitful discussions.

References

[1] Z. Xu, Z. Lin, Coord. Chem. Rev. 156 (1996) 139.
[2] T.J. Marks, J.R. Kolb, Chem. Rev. 77 (1977) 263.
[3] A. Lledos, M. Duran, Y. Jean, F. Volatron, Inorg. Chem. 30 (1991) 4440.
[4] M. Mancini, P. Bougeard, R.C. Burns, M. Mlekuz, B.G. Sayer, J.I.A. Thompson, M.J. McGlinchey, Inorg. Chem. 23 (1984) 1072.
[5] A.P. Hitchcock, N. Hao, N.H. Werstiuk, M.J. McGlinchey, T. Ziegler, Inorg. Chem. 21 (1982) 793.
[6] D.G. Musaev, K. Morokuma, Organometallics 14 (1995) 3327.
[7] S.W. Kirtley, M.A. Andrews, R. Bau, G.W. Grynkewich, T.J. Marks, D.L. Tipton, B.R. Whittlesey, J. Am. Chem. Soc. 99 (1977) 7154.
[8] M.Y. Darensbourg, R. Bau, M.W. Marks, R.R. Burch Jr., J.C. Deaton, S. Slater, J. Am. Chem. Soc. 104 (1982) 6961.
[9] J.C. Bommer, K.W. Morse, J. Chem. Soc. Chem. Commun. (1977) 137.
[10] C. Kutal, P.A. Grutsch, J.L. Atwood, R.D. Rogers, Inorg. Chem. 17 (1978) 3558.
[11] F.-C. Liu, J. Liu, E.A. Meyers, S.G. Shore, Inorg. Chem. 38 (1999) 2169.
[12] E.B. Lobkovskii, A.N. Chekhlov, V.D. Makhaev, A.P. Borisov, Koord. Khim. 15 (1989) 377.
[13] J.A. Jensen, G.S. Girolami, J. Am. Chem. Soc. 110 (1988) 4450.
[14] J.A. Jensen, G.S. Girolami, Inorg. Chem. 28 (1989) 2107.
[15] R. Bau, H.S.H. Yuan, M.V. Baker, L.D. Field, Inorg. Chim. Acta 114 (1986) L27.
[16] T. Kakizawa, Y. Kawano, M. Shimoi, Organometallics 20 (2001) 3211.
[17] T. Yasue, Y. Kawano, M. Shimoi, Angew. Chem., Int. Ed. 42 (2003) 1727.
[18] (a) K. Katoh, M. Shimoi, H. Ogino, Inorg. Chem. 31 (1992) 670;
(b) M. Shimoi, K. Katoh, H. Ogino, J. Chem. Soc., Chem. Commun. (1990) 811.
[19] M. Shimoi, S.-I. Nagai, M. Ichikawa, Y. Kawano, K. Katoh, M. Uruichi, H. Ogino, J. Am. Chem. Soc. 121 (1999) 11704.
[20] (a) A.D. Becke, Phys. Rev. A 38 (1988) 3098;
(b) J.P. Perdew, Phys. Rev. B 33 (1986) 8822;
(c) J.P. Perdew, Phys. Rev. B 34 (1986) 7406.
[21] P.C. Hariharan, J.A. Pople, Theor. Chim. Acta 28 (1973) 213.
[22] P.J. Hay, W.R. Wadt, J. Chem. Phys. 82 (1985) 299.
[23] M.J. Frisch, G.W. Trucks, H.B. Schlegel, G.E. Scuseria, M.A. Robb, J.R. Cheeseman, V.G. Zakrzewski Jr., J.A. Montgomery, R.E. Stratmann, J.C. Burant, S. Dapprich, J.M. Millam, A.D. Daniels, K.N. Kudin, M.C. Strain, O. Farkas, J. Tomasi, V. Barone, M.C.R. Cossi, B. Mennucci, C. Pomelli, C. Adamo, S. Clifford, J. Ochterski, G.A. Petersson, P.Y. Ayala, Q. Cui, K. Morokuma, D.K. Malick, A.D. Rabuck, K. Raghavachari, J.B. Foresman, J. Cioslowski, J.V. Ortiz, A.G. Baboul, B.B. Stefanov, G. Liu, A. Liashenko, P. Piskorz, I. Komaromi, R. Gomperts, R.L. Martin, D.J. Fox, T. Keith, M.A. Al-Laham, C.Y. Peng, A. Nanayakkara, C. Gonzalez, M. Challacombe, P.M.W. Gill, B. Johnson, W. Chen, M.W. Wong, J.L. Andres, C. Gonzalez, M. Head-Gordon, E.S. Replogle, J.A. Pople, GAUSSIAN 98 Revision A.7, Gaussian, Inc., Pittsburgh, PA, 1998.
[24] A.E. Reed, L.A. Curtiss, F. Weinhold, Chem. Rev. 88 (1988) 899.
[25] K.B. Wiberg, Tetrahedron 24 (1968) 1083.
[26] E.D. Glendening, A.E. Read, J.E. Carpenter, F. Weinhold, NBO (version 3.1), Gaussian Inc, Pittsburg, PA, 1998.
[27] S.F. Boys, F. Bernardi, Mol. Phys. 19 (1970) 553.
[28] A. Ariafard, R. Fazaeli, H.R. Aghabozorg, M. Monajjemi, J. Mol. Struct. (Theochem) 625 (2003) 305.
[29] Z. Xu, Z. Lin, Inorg. Chem. 35 (1996) 3964.
[30] R.W. Parry, G. Kodama, Coord. Chem. Rev. 128 (1993) 245.
[31] W. Kutzelnigg, Angew. Chem., Int. Ed. 23 (1984) 272.
[32] H.A. Bent, Chem. Rev. 61 (1961) 275.
[33] A. Ariafard, M.M. Amini, J. Organomet. Chem., in press.
[34] S.P. Walch, C.W. Bauschlicher Jr., in: R. Bartlett (Ed.), Comparison of Ab Initio Quantum Chemistry with Experiment, Reidel, Boston, MA, 1985, p. 17.
[35] G. Frenking, N. Fröhlich, Chem. Rev. 100 (2000) 717.
[36] M. Ingleson, N.J. Patmore, G.D. Ruggiero, C.G. Frost, M.F. Mahon, M.C. Willis, A.S. Weller, Organometallics 20 (2001) 4434.
[37] M. Shimoi, K. Katoh, Y. Kawano, G. Kodama, H. Ogino, J. Organomet. Chem. 659 (2002) 102.